Title

Thermal fracture kinetics of heterogeneous semiflexible polymers

Journal

Soft Matter, 16(8)

ISSN

1744-683X

Authors

Lorenzo, Alexander M
De La Cruz, Enrique M
Koslover, Elena F

Publication Date

2020-02-26

DOI

10.1039/c9sm01637f

Peer reviewed

HHS Public Access

Author manuscript

Soft Matter. Author manuscript; available in PMC 2021 February 26.

Published in final edited form as:

Soft Matter. 2020 February 26; 16(8): 2017–2024. doi:10.1039/c9sm01637f.

Thermal Fracture Kinetics of Heterogeneous Semiflexible Polymers

Alexander Lorenzo[1], **Enrique M. De La Cruz**[2], **Elena F. Koslover**[1,*]

[1]Department of Physics, University of California, San Diego, San Diego, California 92093

[2]Department of Molecular Biophysics and Biochemistry, Yale University, New Haven, CT 06520

Abstract

The fracture and severing of polymer chains plays a critical role in the failure of fibrous materials and the regulated turnover of intracellular filaments. Using continuum wormlike chain models, we investigate the fracture of semiflexible polymers via thermal bending fluctuations, focusing on the role of filament flexibility and dynamics. Our results highlight a previously unappreciated consequence of mechanical heterogeneity in the filament, which enhances the rate of thermal fragmentation particularly in cases where constraints hinder the movement of the chain ends. Although generally applicable to semiflexible chains with regions of different bending stiffness, the model is motivated by a specific biophysical system: the enhanced severing of actin filaments at the boundary between stiff bare regions and mechanically softened regions that are coated with cofilin regulatory proteins. The results presented here point to a potential mechanism for disassembly of polymeric materials in general and cytoskeletal actin networks in particular by the introduction of locally softened chain regions, as occurs with cofilin binding.

Graphical Abstract

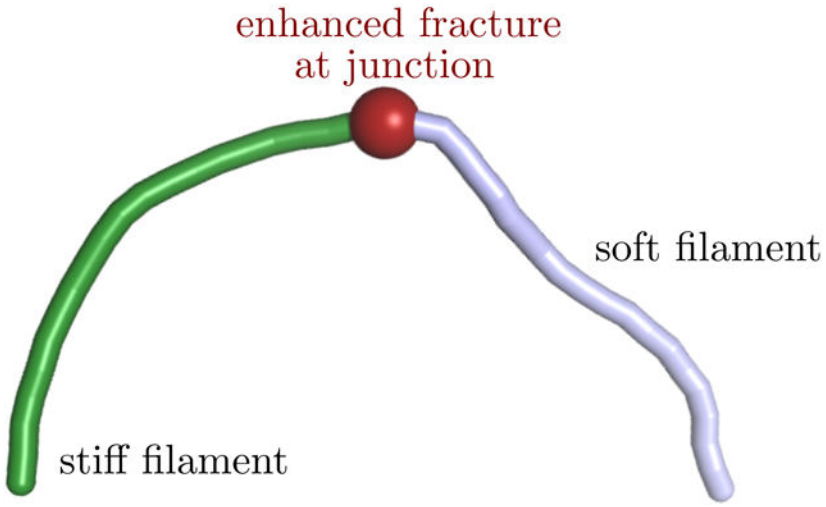

A kinetic model for fracture of heterogeneous semiflexible polymers, such as cofilin-coated actin filaments, shows that mechanical heterogeneity enhances fracture rates.

* ekoslover@ucsd.edu.

1. INTRODUCTION

The fracture properties of polymeric solids pose a key constraint on the manufacture and design of a vast array of man-made materials for load-bearing or weather-resistant purposes[1, 2]. Furthermore, polymeric materials serve as some of the most important structural and information-bearing components in living organisms, and their rupture (whether through mechanical or environmental stress or through regulated turnover) has a crucial role to play in biological processes ranging from cell division[3], to tumorigenesis[4], to cell motility[5]. Theoretical and experimental explorations of failure mechanisms have established that the fracture of polymeric solids relies in large part on the scission of individual polymer filaments, with the dynamics and stress-dependence of fracture governed by the kinetics of molecular rupture[1, 6, 7]. At the molecular scale, fracture is inherently a thermal process, where the activation energy is lowered by the application of stress on individual bonds along the filament[7].

Fragmentation of a polymer filament is accelerated when externally applied stresses become locally concentrated in specific regions. This principle underlies, for instance, the fragmentation of DNA at discrete folding points under extensional flow[8], the rupture of microtubules through buckling during spindle reorganization[9] and traumatic axonal injury[10], and the severing of actin bundles by myosin-driven compression in motile cells[11, 12]. Local discontinuities in mechanical properties tend to concentrate externally applied stress, leading to preferential fracture of materials at these discontinuous regions[13, 14].

In the case of thermally driven fracture, the effect of mechanical inhomogeneities in a filament is poorly understood. Prior theoretical work showed that thermal energy is equally partitioned among spatial degrees of freedom in general equilibrium one-dimensional systems[15]. However, fracture is inherently a transient, kinetic process. Understanding fracture rates requires moving beyond equilibrium distributions to consider the dynamics of thermal fluctuations in a polymer filament. Here we focus on the role of spatial heterogeneity of mechanical properties in accelerating thermally induced fracture of semiflexible chains.

The general problem of fracture rates in a thermalized, mechanically heterogeneous, polymer filament is motivated in part by a biological system: the cofilin-mediated severing of cytoskeletal actin filaments. Actin is a semiflexible polymer that forms bundles and networks responsible for maintaining cell-scale mechanical properties as well as driving processes such as lamellipodial motility, cytokinesis, and embryonic patterning[16, 17]. Much of the biological behavior of actin networks relies on the dynamic turnover of individual actin filaments, which is accelerated by the actin-binding protein cofilin. Cofilin assembles cooperatively along actin chains, locally decreasing their bending stiffness and resulting in mechanically heterogeneous partially decorated filaments[18-22]. Such filaments fragment, without additional energy input, preferentially at the boundary of cofilinated segments[21, 23, 24]. While missing bonds at these discontinuities may account for their increased fragility, particularly under stress[25], an additional contribution to

enhanced severing has been proposed that relies on the concentration of stress at the discontinuities between cofilinated and bare actin segments[14, 25].

Here, we explore the physical plausibility of enhanced fracture at a junction between soft and stiff regions, in a purely thermal system (ie: with zero average force applied to the chain ends). Our focus is first on the limit where the dynamics of the junction are very fast compared to the slow equilibration of the full chain configuration. In the case of slowly-moving or constrained chain ends we show that mechanical heterogeneity can increase fracture rates by orders of magnitude. Furthermore, we show that even in the case of freely equilibrating chains, the separation in time-scales between local junction equilibration and whole chain rearrangement results in modest acceleration of fracture in heterogeneous as compared to homogeneously stiff chains.

2. MECHANICAL MODEL FOR HETEROGENEOUS FILAMENT

We consider the thermally driven fracture of a mechanically heterogeneous filament, by building upon the well-established continuum “worm-like chain” (WLC) model for semiflexible polymers[26, 27]. Prior work on the statistical mechanics of heterogeneous and kinked worm-like chains has established a framework for analytically calculating their distribution functions[28-30]. Here we focus on the simplest heterogeneous chain: a diblock copolymer consisting of two WLC of equal length L and bending persistence lengths $\ell_{p,1} \geq \ell_{p,2}$. The chains are grafted together at a point junction (Fig. 1a), whose bending energy is defined as

$$\frac{1}{k_b T} E_{\text{junc}} = \kappa(1-\rho), \qquad \rho = \cos\theta, \tag{1}$$

where $k_b T$ is the thermal energy and θ is the bending angle between chain tangents at the junction. The junction represents a short portion of the chain of length Δ, with $\Delta \ll L$. In our model, this junction is treated as a single point with stiffness $\kappa = \ell_{p,1}/\Delta$. In particular, we note that this junction represents the behavior of the last short segment of stiff chain just before the attachment of the softer chain.

The mechanics of the heterogeneous chain are fully defined by three dimensionless parameters: chain halflength $N = L/(2\ell_{p,1})$, junction length $\widehat{\Delta} = \Delta / L = 1/(2\kappa N)$, and heterogeneity $h = \ell_{p,1}/\ell_{p,2}$.

The overall partition function $[G_{\text{tot}}(\vec{R}, \rho)]$ for this model is computed from prior results derived for wormlike chains with end constraints[27, 30, 31]. We start with the partition function $[\widehat{G}(\vec{R}, \vec{u}; L, \ell_p)]$ for a WLC chain of length L, persistence length ℓ_p, with one end at the origin, the other end at position $\vec{R}$, and final end tangent $\vec{u}$. After a Fourier transform from $\vec{R}$ to $\vec{k}$, this function is given by:

$$\hat{G}(\vec{k},\vec{u};L,\ell_p)=\frac{1}{4\pi}\sum_{l=0}^{\infty}\mathcal{G}_{0,l}\left(2\ell_p k,\frac{L}{2\ell_p}\right)P_l(\vec{u}\cdot\vec{k}), \tag{2}$$

where P_l are Legendre polynomials and the $\mathcal{G}^m_{l_0,l_f}$ coefficients refer to previously defined continued fraction terms[27]. For a heterogeneous wormlike chain with end-to-end vector $\vec{R}$ and junction angle θ, the partition function is obtained from the convolution of two such propagators

$$\begin{aligned}G_{\mathrm{tot}}(\vec{R},\rho;L,\ell_{p,1},\ell_{p,2})=\int d\vec{R}_j d\vec{u}_j d\phi\hat{G}(\vec{R}_j,\vec{u}_j;L,\ell_{p,1})\\ \times\hat{G}(\vec{R}-\vec{R}_j,\boldsymbol{\Omega}(\theta,\vec{\phi})\cdot u_j;L,\ell_{p,2})\end{aligned} \tag{3}$$

where $\vec{R}_j$ is junction position, $\vec{u}_j$ is the incoming tangent to the junction, and $\Omega(\phi, \theta)$ is a rotation matrix that rotates the cannonical coordinate system by Euler angles $(\phi, \theta, 0)$. The Fourier transform in space, together with an application of the spherical harmonic addition theorem[32], allows this convolution to be simplified to:

$$\hat{G}_{\mathrm{tot}}(\vec{k},\rho;N,1,h)=\frac{1}{2}\sum_{\ell=0}^{\infty}P_l(\rho)\mathcal{G}_{0,l}(k,N)\,\mathcal{G}_{0,l}\left(\frac{k}{h},hN\right), \tag{4}$$

where we have nondimensionalized all length units by $2\ell_{p,1}$. Finally, the Fourier inversion is computed according to[31]

$$\begin{aligned}&G_{\mathrm{tot}}(\vec{R},\rho;N,1,h)=\\ &\frac{1}{(2\pi^2)(2\ell_{p,1})^3}\int_0^{\infty}dk\frac{k\sin(2kNr)}{2Nr}\hat{G}_{\mathrm{tot}}(k,\rho;N,1,h),\end{aligned} \tag{5}$$

where $r=|R|/(2L)$ is the normalized end separation of the joint chain. This propagator is normalized such that $\int d\vec{R}\,G_{\mathrm{tot}}(\vec{R},\rho)=1$ for each value of ρ.

The free energy (F) of the chain is then defined as the log of the partition function, with an additional term for the bending of the junction angle. Namely,

$$\frac{1}{k_bT}F(r,\rho)=\kappa(1-\rho)-\log\left[r^2G_{\mathrm{tot}}(r,\rho)\right] \tag{6}$$

This free energy landscape is plotted in Fig. 1 for a homogeneous, stiff chain and a heterogeneous chain. The example filaments in Fig. 1a,c correspond to the lowest energy (zero-temperature) configurations for both the homogeneous and heterogeneous chains with end separation fixed at $r = 0.6$. These configurations are qualitatively similar to those previously observed for athermal models of bare and partially cofilinated actin[14, 25], with the most pronounced bending on the softer side of the chain, close to the junction. We note, however, that the minimal free energy associated with a given end distance (Fig. 1b,d) typically occurs at much steeper junction bending angles than the athermal configuration,

due to the entropic favorability of bending. Thus, the inclusion of thermal fluctuations in our model fundamentally alters the behavior of the chain, as compared to previous athermal models.

We focus on filament fracture at the junction point, assuming that fracture will occur when thermal fluctuations push the junction energy (E_{junc}) above some predefined cutoff (E^*). This model represents a fracture process where the junction itself must hop over a transition energy barrier, with the cosine of the bending angle ρ as the reaction coordinate. Chains with a more flexible junction (lower κ) must reach more extreme junction bending ($\rho^* = 1 - E^*/\kappa$) than chains with a stiffer junction (higher κ). The model formulation is consistent with previous analyses of experimental data on fracture of short cofilin-decorated actin filaments that points to fracture occuring beyond a critical bending angle that increases with lower filament persistence length[21]. Critical energies of approximately 22kT have been estimated for the severing of bare actin filaments[21].

The overall rate of fracture is obtained from the mean first passage time (MFPT) to the critical value ρ^*, as the system fluctuates thermally over the free energy landscape plotted in Fig. 1. The kinetics of fracture are thus determined by a free energy barrier incorporating both the junction bending energy and the configurational free energy of the worm-like chains. For a homogeneously stiff chain, surmounting this barrier along the minimum energy path requires bringing the ends of the chain closer together (Fig. 1b). For the heterogeneous chain, by contrast, the cutoff junction angle can be reached without substantial change in the end-to-end distance (Fig. 1d). The importance of this effect in determining the overall time to fracture depends on the dynamics of the end-to-end coordinate r compared to the dynamics of the junction angle.

3. DYNAMICS OVER FREE ENERGY LANDSCAPE

The free energy landscapes of Fig. 1, in and of themselves, define only the equilibrium distribution of the chain. Establishing the timescale for fracture requires consideration of the dynamics of a heterogeneous WLC through its configurational space. An exact analytical treatment of WLC dynamics would require resolving the movement of all its dynamic modes[33], which couple together in a complex way to determine the evolution of observable parameters such as chain end-to-end distance or a local bending angle. Instead, we simplify the dynamics of the system by treating it as an effective diffusion-limited kinetic process over a two-dimensional landscape. This approach relies on the approximation that intermediate chain modes relax rapidly compared to the overall reaction time for fracture, but that the longest mode (which sets the chain end-to-end distance) may relax more slowly than this time-scale. In fact, as seen below, fracture enhancement for a heterogeneous chain occurs only when chain end equilibration is slower than the fragmentation, either due to external constraints (*eg:* for cross-linked or entangled filaments) or for intermediate cutoff energies.

An analogous approach, mapping to a one-dimensional effective free energy landscape, has previously been employed by many groups in estimating the looping time of semiflexible chains[34-37]. Such models rely on the approximation that the intermediate degrees of

freedom in the chain equilibrate rapidly compared to the reaction time of interest, allowing the dynamical system to be approximated as diffusion to capture over an effective reaction coordinate. While the general validity of such an approach has recently been called into question[38], comparison of looping time between Brownian Dynamics simulations and effective kinetic models have been shown to have good agreement in the regime where the chain is short ($N < 2$) and not tightly bent (end-to-end distance greater 10% of the chain length), provided an appropriate dynamic prefactor is selected in the kinetic models[38]. In the current work, we use comparison with Brownian Dynamics simulations to directly validate the approximate kinetic model.

In our model, polymer fracture is defined by a transition in a rapidly-equilibrating degree of freedom: the bending angle of the junction. We thus rely on a separation of timescales between movement along the two dimensions of the free energy landscape. For each value of the chain end distance r, the kinetics of transition to the cutoff ρ^* are approximated as being described by a single time scale – the mean first passage time $\tau(\rho^*; r)$ along a horizontal slice of the landscape. Dynamics along the angular coordinate are defined by a variable friction coefficient that depends on the value of the junction angle,

$$\zeta(\rho) = \frac{k_B T}{D_\rho^{(0)}} \frac{5 - 3\rho}{6(1 - \rho^2)} \tag{7}$$

where $D_\rho^{(0)} = \frac{k_B T}{\mu \Delta^3}$ and μ is the translational friction coefficient per unit length of the chain. This expression is derived from the dynamics of two connected rigid links (Appendix A). The prefactor $D_\rho^{(0)}$ captures the rapid dynamics of the short chain region represented by the junction and does not depend on the overall length of the chain (Supplemental Figure S1). We note that the numerical prefactor in the friction coefficient (Eq. 7) depends on mapping from the behavior of two rigid links to the dynamics of a point-like kink representing a short length of semiflexible chain. This prefactor is not directly determined by our theory, and we fit the appropriate length of links to establish this mapping (specifically, $\ell_{\text{link}} = 2\Delta$) by matching the theory to Brownian dynamics simulations of semiflexible chains, as described below. This is the only fitting parameter in the model; a single value (shown in Eq. 7) is used for all subsequent results described.

It should be noted that the time to reach a cutoff junction angle for a fixed end-to-end distance cannot be obtained by mapping to Kramers' classic transition rate theory[39] as this event does not constitute passage across a high transition barrier. In fact, as can be observed in Fig. 1a, when the end-to-end distance is fixed to intermediate values (*eg*: $r = 0.5$) then moving towards smaller junction angles actually entails a decrease in the free energy of the entire chain, while generating a high bending energy E_{junc} at the junction itself. Consequently, we take a more generally applicable approach for calculating first passage times on a one-dimensional landscape[40].

Our calculations assume that the chain configuration starts at thermal equilibrium, and that those chains with a junction angle beyond the fracture cutoff ($\cos\theta < \rho^*$) have a fracture time of zero. The mean first passage time over the free energy landscape with fixed r can be

computed from the Fokker-Planck equation[40-43], appropriately modified for spatially varying diffusivity[44] (Appendix B). Specifically, the fracture time for a fixed value of r is given by

$$\tau(\rho^*, r) = \frac{1}{\int_0^1 e^{-F(r,\rho)/k_bT} d\rho} \times \times \left[\int_{\rho^*}^1 d\rho \int_{\rho^*}^{\rho} d\rho' \int_{\rho'}^1 d\rho'' \frac{\zeta(\rho')}{k_bT} e^{(F(r,\rho') - F(r,\rho'') - F(\rho))/k_bT} \right]. \quad (8)$$

Brownian dynamics simulations of a discretized WLC model (details in Appendix D) are used to validate our calculations of the mean first passage time for fixed values of the end distance, with the free energy landscape given by Eq. 6 and the friction coefficient in Eq. 7. As shown in Fig. 2a, the continuum chain theory accurately reproduces the kinetics of reaching a high junction angle in simulations.

The overall mean first passage time to fracture can be computed by considering a system that fluctuates over discrete states in the normalized end distance, with state i corresponding to $r_i = i\delta r$, and the discretization set to $\delta r = 0.01$. The system is assumed to start in thermal equilibrium, with the probability of starting in state i set by a Boltzmann factor corresponding to the free energy of that state: $F_i = -k_BT \log \int d\rho \exp[-F(r_i,\rho)/k_BT]$.

To calculate kinetics on a complex energy landscape, a well-established approach is to assume Markovian (memory-less) transitions between neighboring states with the transition rate depending on the energy difference between each pair of states. The appropriate transition rates can be extracted from a discretization of the Fokker-Plank equation[45, 46]. Specifically, transitions between states in our model occur with rate constants $k_i^{(\pm)}$, given by

$$k_i^{(\pm)} = \frac{\frac{k_R}{\delta r^2}(F_{i\pm1} - F_i)}{\exp(F_{i\pm1} - F_i) - 1}. \quad (9)$$

The dynamic prefactor is taken to be the time-scale for three-dimensional translational diffusion of a chain of length L over a length scale $\Delta R = 2L\delta r$, according to:

$$\frac{k_R}{\delta r^2} = \frac{6k_BT}{(\mu L)(2L\delta r)^2}. \quad (10)$$

This approximate model for the dynamics of the chain ends allows for analytical calculation of a mean first passage time to an arbitrary value of the normalized end separation r. Specifically, the distribution of times to move from any starting state i to any final state j can be obtained by convolving together Poisson processes representing individual Markovian steps with rate constants given by Eq. 9. Summing over all possible paths from a given starting state to a specific end separation r then allows extraction of the mean first passage time (details in Appendix C). This approach can be applied to exploring the dynamic properties of any system described by an arbitrary network of states with memory-less

transitions between them[47, 48], and has been extensively employed for analyzing complex molecular transitions under the name of “Markov state models”[49] or “discrete path sampling”[50]. The resulting mean first passage times to a cutoff end-to-end distance are comparable to those found with Brownian dynamics simulations of chains that are initiated with configurations sampled from thermal equilibrium (Fig. 2b).

To put together both dimensions of the energy landscape, we treat fracture as a Poissonian process within each particular end-distance state, with average time given by $\tau_i = \tau(\rho^*, r_i)$. The dynamics of fracture can then be thought of as transitions between discrete states (r_i) on a one-dimensional landscape, with a different rate ($1/\tau_i$) of reaching the final fractured state from each of these discrete r states. We compute the overall mean time to fracture for such a system using well-established methods for extracting low-order moments of transition times on a network of arbitrarily connected states[47, 48] (see Appendix C).

The use of a single timescale τ_i for the fracture transition at each end separation is a simplifying approximation that relies on the assumption of well-separated time-scales. Namely, we assume that the bending dynamics of the short junction region are very fast compared to motion of the chain ends, making it possible to treat each transition between r_i states as memory-less. This approximate approach for representing the dynamics of the system is validated by comparison to Brownian dynamics simulations with unconstrained homogeneous chains (Appendix D; Supplemental Video 1). As shown in Fig. 2c, our model of dynamic fluctuations over a two-dimensional energy landscape with well-separated time scales can accurately represent the transition to fracture for simulated chains.

4. FRACTURE RATES FOR HETEROGENEOUS CHAINS

The overall time to fracture is dependent on the relative rate of motion in the end-to-end distance as compared to the rate of junction fluctuations (Fig. 3a). For the case of very rapid end equilibration (high $k_R / D_\rho^{(0)}$), the chain would be expected to sample all end positions over a time-scale that is short compared to the fracture time. In this limit, the fracture dynamics are determined entirely by the stiffness and friction coefficient for the junction bending (ρ) and are independent of the mechanical properties of the rest of the chain.

The opposite regime holds when the dynamics of the end distance are much slower than those of the junction angle. In this case, the end distance remains constant at its starting value, and the mean time to fracture is the weighted average of the individual τ_i. Softer mechanics in one half of the chain make it more probable that a lower value of r will initially be selected from the equilibrium distribution. This lower r persists over time and allows the junction to more rapidly reach the cutoff angle.

Fig. 3b,c show the mean time to fracture for chains with different degrees of heterogeneity h in the case of fixed end-to-end distance (infinitely slow r dynamics). In this limit, a purely stiff chain will be slow to reach fracture at the junction because a higher overall chain deformation energy is required to bend the junction to the point of fracture. A purely soft chain will also be slow to reach fracture because the requisite junction angle θ^* to achieve the same cutoff energy will be correspondingly larger[21]. Rapid fracture can be achieved by

a heterogeneous chain, where the junction stiffness and hence the cutoff angle are set by the stiff side of the chain, while the low persistence length of the soft side enables the junction to reach that cutoff angle without moving the chain ends or incurring a substantial cost in chain deformation energy. The enhancement due to chain heterogeneity can reach several orders of magnitude in cases where the junction must reach very steep bending angles in order to fracture (high N and $\widehat{\Delta}$).

In the case where chain ends are unconstrained, the importance of chain heterogeneity depends on the relative time-scales of junction bending versus the longest equilibration time for the chain. Specifically, heterogeneity can enhance fracture when the time for the junction to reach the cutoff energy E^* is lower than the full chain equilibration time. In this regime, the chain ends do not have the opportunity to sample the full configurational space, and the ability of a heterogeneous chain to reach the bending cutoff with less change in the end-to-end distance leads to faster fracture (Fig. 4). This situation is analogous to the “diffusion-controlled” regime identified for polymer looping[51], where a reaction occurs on a timescale smaller than the chain equilibration time. Because the time to fracture increases exponentially with E^*, at high values of the cutoff energy the difference between heterogeneous and homogeneous chains disappears. For large E^*, the entire chain has time to equilibrate before fracture occurs, putting it into the “meanfield” regime[51] where reaction rates are determined by the equilibrium distribution of the chain. By, contrast when E^* becomes low, very little change in the end-to-end distance is necessary to reach the cutoff for fracture, as seen in the free energy landscape of Fig. 1b. In effect, sufficient junction bending can be attained by small amplitude fluctuations in higher order modes. Because our energy-landscape picture assumes that these higher order modes are equilibrated, the dependence on chain stiffness heterogeneity disappears when the cutoff angle is small. Consequently, a local maximum is observed in the ratio of fracture times for heterogeneous versus homogeneous chains with respect to the cutoff energy E^* (Fig. 4). While our kinetic model makes the fundamental simplifying approximation of equilibrated higher-order modes, qualitatively similar behavior for stiff versus heterogeneous chains is observed in Brownian Dynamics simulations (Supplemental Fig. S4; Supplemental Video 2).

The dimensionless parameter describing the relative rates of junction dynamics versus whole-chain equilibration is $k_R / D_\rho^{(0)} = \frac{3}{2}\widehat{\Delta}^3$. In order for heterogeneity to affect fracture rate, this parameter must be sufficiently small – allowing the junction to sample over many bending angles before the chain ends can equilibrate. Small values of $\widehat{\Delta}$ require a combination of short junction length-scale (corresponding to high junction modulus κ) and/or long chain lengths (high N). Decreasing $\widehat{\Delta}$ by increasing κ implies that the same junction cutoff energy corresponds to a less steep cutoff angle and a smaller time to fracture. Consequently, the value of E^* at which the fracture time begins to compete with the equilibration time of the entire chain is increased, and the curves of $\tau_{\text{stiff}}/\tau_{\text{het}}$ shift to the right (Fig. 4a). In the limit of high κ, the fracture process is dominated by the junction bending and the mechanical properties of the rest of the chain cease to matter. Similarly, if we decrease $\widehat{\Delta}$ by lengthening the chain, the local maximum with respect to E^* moves to the right (Fig. 4b), as higher cutoff energies can be reached in a timescale comparable to the full chain equilibration. The increased flexibility of the stiff side of the chain in this case

obviates the difference between the heterogeneous and homogeneous chains, an effect that may directly result from the approximation that intermediate chain modes are fully equilibrated. Due to the limitations of this approximation, the behavior of the fracture rate with chain length may not be well resolved in our model for longer chains (especially when the softer side of the chain exceeds $hN \gg 2$). However the qualitative effect remains – heterogeneity in the chain mechanics increases the rate of fracture, up to approximately 15%, in the regime when the full chain cannot equilibrate on time-scales comparable to the fracture time.

5. CONCLUDING REMARKS

Our calculations show that filament heterogeneity can substantially enhance the rate of thermal fracture in the case of restricted end-to-end dynamics of the filament. A modest enhancement is expected for the case of a chain with freely moving ends. We note that the model developed here differs from previous athermal models for fracture[14, 25] which indicated that a heterogeneous chain concentrates stresses at the junction when the chain is forced into a buckled configuration. The enhancement in thermally driven fracture occurs despite the fact that the initial configuration of the chain is allowed to sample from the equilibrium distribution. The contrast between the case of rapid and slow r equilibration (Fig. 3a) highlights the purely dynamic nature of this effect. Fracture enhancement arises from the separation in time-scales between fluctuations at the junction versus moving the ends of the entire polymer. The presence of a softer chain region allows a junction to reach steep bending angles without requiring large movements of the chain ends and without paying a large energetic cost for the chain deformation.

Our results thus highlight fracture as an inherently dynamic, non-equilibrium process. Despite the fact that the time-averaged distribution of junction angles obeys Boltzman statistics regardless of the mechanical properties of the rest of the chain, the time for that junction to first pass a cutoff angle depends on the time-scales associated with moving both the junction itself and the longer stretches of chain surrounding it. Thus, a difference between heterogeneous and homogeneous chains is observed even though the starting distribution of junction angles is taken from equilibrium, both in the case of free chain ends and in the situation where chain ends are fixed to highlight the limit of slow end equilibration.

A fundamental simplifying approximation in our model relies on the separation of time-scales for the dynamics of different modes in a fluctuating filament. Namely, we treat the slowest mode, corresponding to the chain end-to-end distance, as an explicit coordinate for our analytic model. All higher-order modes are assumed to equilibrate rapidly, allowing the definition of a free energy landscape (Fig. 1). This approximation neglects the broad range of time-scales corresponding to the intermediate modes, which lead to subdiffusive Rouse dynamics for times shorter than the equilibration of the entire chain[52]. Past theoretical work on intramolecular reaction rates within long flexible polymer chains has shown that inclusion of the full range of dynamic modes is necessary in order to correctly predict the scaling of reaction times with chain size or capture radius[51, 53]. For instance, cyclization rates for such chains are not well-predicted by mapping to an effective harmonic potential

which describes the free energy of a Gaussian chain[54]. For semiflexible chains, mapping to an effective free energy landscape by integrating over all intermediate modes has been employed in a number of studies focusing on chain looping[34-37]. A recent overview[38] has shown that for these chains, as well, mapping to a one-dimensional landscape leads to incorrect behavior of the model in several asymptotic limits. However, for short, stiff chains with relatively large end-to-end distances, good agreement of the approximate landscape model with explicit Brownian Dynamics simulations can be achieved[38]. Here, we are working precisely in this regime, as evidenced by the agreement of our approximate model with simulations (Fig. 2). Thus, we do not make predictions of the fragmentation time scaling behavior, but rather focus on the important qualitative conclusion that mechanical heterogeneity in the chain can enhance fracture rates, even when the chain ends are unconstrained. Such enhancement relies on the time-scale of fragmentation being faster than the relaxation time of the full chain. These qualitative results are further supported by simulations of heterogeneous chains with free ends (Supplemental Fig. S4).

The model with restricted chain ends, where fracture enhancement is especially pronounced, is particularly relevant for the cofilin-mediated severing of actin filaments within a cytoskeletal network. In such networks cross-links and entanglements can effectively restrict the movement of certain positions along the chain, while allowing rapid equilibration of chain positions between the crosslink points. Our results indicate that in such situations introducing mechanical heterogeneity into the actin filaments by cofilin binding should substantially increase thermal severing rates.

It should be noted that, in addition to changing the flexibility of actin filaments, cofilin binding also alters the filament twist density. Recent experiments have shown that constraining filaments to prevent torsional equilibration enhances actin filament severing by cofilin [24, 55, 56]. The effect described here centers on severing due to bending fluctuations and may provide a parallel, unrelated mechanism for cofilin-driven fracture. Both twist-based and bending-based severing are expected to depend on the density and mechanics of cross-links in an actin network. By providing a feedback mechanism between network structure and actin severing dynamics, these physical effects may play an important role in regulating the self-assembly, turnover, and mechanoresponse of cytoskeletal structures.

In addition to helping unravel the mechanisms of actin severing by cofilin, the results presented here are generally applicable to the fracture of any semiflexible thermally fluctuating polymer. Enhanced rates of thermally-activated fracture in mechanically heterogeneous chains point towards general principles for controlling the stability of nanoscale systems, including polymer networks, nanotubules, and molecular threads, for a broad range of biological and industrial applications.

Supplementary Material

Refer to Web version on PubMed Central for supplementary material.

ACKNOWLEDGMENTS

The authors thank R. Phillips, H. Garcia, J. Kondev, and J. Theriot for organizing the Physical Biology of the Cell course, whence this collaboration originated. Funding was provided by the Alfred P. Sloan Foundation Fellowship (E.F.K.), the William A. Lee Undergraduate Research Award (A.L.) and NIH grant R01-GM097348 (E.D.L.C).

References

[1]. Kausch H-H, Polymer fracture, volume 2, Springer Science & Business Media, 1987.

[2]. Ward IM and Sweeney J, Mechanical properties of solid polymers, John Wiley & Sons, 2012.

[3]. Zhou X et al., Science 348, 574 (2015). [PubMed: 25931560]

[4]. van Gent DC, Hoeijmakers JH, and Kanaar R, Nat Rev Genet 2, 196 (2001). [PubMed: 11256071]

[5]. Pollard TD and Borisy GG, Cell 112, 453 (2003). [PubMed: 12600310]

[6]. Regel VR, Slutsker AI, and Tomashevskii EE, Physusp+ 15, 45 (1972).

[7]. Tomashevskii E et al., Int J Fracture 11, 803 (1975).

[8]. Reese HR and Zimm BH, J Chem Phys 92, 2650 (1990).

[9]. Schiel JA et al., J Cell Sci 124, 1411 (2011). [PubMed: 21486954]

[10]. Tang-Schomer MD, Patel AR, Baas PW, and Smith DH, Faseb J 24, 1401 (2010). [PubMed: 20019243]

[11]. Medeiros NA, Burnette DT, and Forscher P, Nat Cell Biol 8, 216 (2006).

[12]. Tsai TY-C et al., Dev Cell 49, 189 (2019). [PubMed: 31014479]

[13]. Suresh S, Science 292, 2447 (2001). [PubMed: 11431558]

[14]. De La Cruz EM, Martiel J-L, and Blanchoin L, Bio- phys J 108, 2270 (2015).

[15]. Bar-Sinai Y and Bouchbinder E, Phys Rev E 91, 060103 (2015).

[16]. Fletcher DA and Mullins RD, Nature 463, 485 (2010). [PubMed: 20110992]

[17]. Salbreux G, Charras G, and Paluch E, Trends Cell Biol 22, 536 (2012). [PubMed: 22871642]

[18]. McGough A and Chiu W, J Mol Biol 291, 513 (1999). [PubMed: 10448032]

[19]. McCullough BR, Blanchoin L, Martiel J-L, and De La Cruz EM, J Mol Biol 381, 550 (2008). [PubMed: 18617188]

[20]. Pfaendtner J, Enrique M, and Voth GA, P Natl Acad Sci 107, 7299 (2010).

[21]. McCullough BR et al., Biophys J 101, 151 (2011). [PubMed: 21723825]

[22]. Fan J et al., J Mol Biol 425, 1225 (2013). [PubMed: 23352932]

[23]. De La Cruz EM, Biophysical reviews 1, 51 (2009). [PubMed: 20700473]

[24]. Elam WA, Kang H, and De La Cruz EM, Febs Lett 587, 1215 (2013). [PubMed: 23395798]

[25]. Schramm AC et al., Biophys J 112, 2624 (2017). [PubMed: 28636918]

[26]. Kratky O and Porod G, Recl Trav Chim Pay-b 68, 1106 (1949).

[27]. Spakowitz AJ and Wang Z-G, Phys Rev E 72, 041802 (2005).

[28]. Wiggins PA, Phillips R, and Nelson PC, Phys Rev E 71, 021909 (2005).

[29]. Zhang H and Marko JF, Phys Rev E 82, 051906 (2010).

[30]. Koslover EF and Spakowitz AJ, Macromolecules 46, 2003 (2013).

[31]. Mehraeen S, Sudhanshu B, Koslover EF, and Spakowitz AJ, Phys Rev E 77, 061803 (2008).

[32]. Arfken G, Weber H, and Harris F, (2005).

[33]. Aragon SR and Pecora R, Macromolecules 18, 1868 (1985).

[34]. Jun S, Bechhoefer J, and Ha B-Y, EPL (Europhysics Letters) 64, 420 (2003).

[35]. Klenin KV and Langowski J, The Journal of chemical physics 121, 4951 (2004). [PubMed: 15332931]

[36]. Hyeon C and Thirumalai D, The Journal of chemical physics 124, 104905 (2006). [PubMed: 16542102]

[37]. Mulligan PJ, Chen Y-J, Phillips R, and Spakowitz AJ, Biophysical journal 109, 618 (2015). [PubMed: 26244743]

[38]. Afra R and Todd BA, The Journal of chemical physics 138, 174908 (2013). [PubMed: 23656160]
[39]. Kramers HA, Physica 7, 284 (1940).
[40]. Szabo A, Schulten K, and Schulten Z, The Journal of chemical physics 72, 4350 (1980).
[41]. Fox RF, Phys Rev A 33, 467 (1986).
[42]. Risken H, Fokker-planck equation, in The Fokker-Planck Equation, pages 63–95, Springer, 1996.
[43]. Koslover EF and Spakowitz AJ, Phys Rev Lett 102, 178102 (2009). [PubMed: 19518837]
[44]. Lau AW and Lubensky TC, Phys Rev E 76, 011123 (2007).
[45]. Wang H, Peskin CS, and Elston TC, J Theor Biol 221, 491 (2003). [PubMed: 12713936]
[46]. Xing J, Wang H, and Oster G, Biophysical journal 89, 1551 (2005). [PubMed: 15994886]
[47]. Masuda N, Porter MA, and Lambiotte R, Physics reports 716, 1 (2017).
[48]. Koslover EF and Spakowitz AJ, Phys Rev E 86, 011906 (2012).
[49]. Chodera JD and Noé F, Current opinion in structural biology 25, 135 (2014). [PubMed: 24836551]
[50]. Wales DJ, Molecular physics 100, 3285 (2002).
[51]. Friedman B and O'Shaughnessy B, International Journal of Modern Physics B 8, 2555 (1994).
[52]. Doi M and Edwards SF, The theory of polymer dynamics, volume 73, Oxford University Press, 1988.
[53]. Doi M, Chemical Physics 9, 455 (1975).
[54]. Sakata M and Doi M, Polymer Journal 8, 409 (1976).
[55]. Pavlov D, Muhlrad A, Cooper J, Wear M, and Reisler E, J Mol Biol 365, 1350 (2007). [PubMed: 17134718]
[56]. Wioland H, Jegou A, and Romet-Lemonne G, P Natl Acad Sci 116, 2595 (2019).

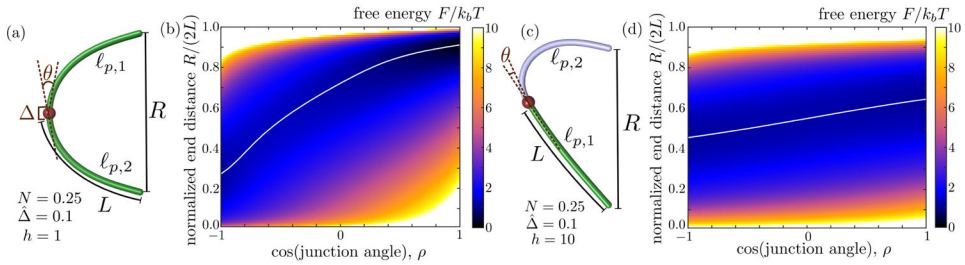

Figure 1.

Model schematic and energy landscapes. (a) Lowest energy (athermal) configuration of homogeneous chain with fixed $R/(2L) = 0.6$ and model parameters labeled. (b) Free energy landscape for homogeneous chain shown in (a), plotted as a function of junction bending and normalized end distance. White line markes the lowest energy path to steeper junction angles. (c) Lowest energy configuration for a heterogeneous chain with fixed $R/(2L) = 0.6$ and $\ell_{p,1}/\ell_{p,2} = 10$. Light blue segment corresponds to softer chain side. (d) Overall free energy landscape for the heterogeneous chain with $h = 10$.

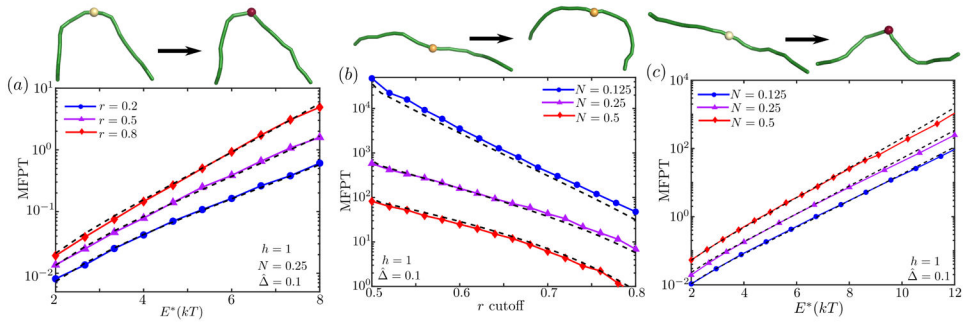

Figure 2.

Comparison of approximate dynamics over free energy landscapes versus Brownian dynamics simulations, for homogeneous chains ($h = 1$). (a) MFPT to a cutoff junction energy E^*, for fixed end distance. (b) MFPT to a cutoff value of the normalized end-to-end distance r. (c) MFPT to a junction energy E^*, with free chain ends. In all cases, dashed black lines correspond to first passage times calculated from the free energy landscapes, solid lines correspond to Brownian dynamics simulations. All times are non-dimensionalized by $D_\rho^{(0)}$. Top panels show examples of start and end configurations, with junction color indicating energy at the junction.

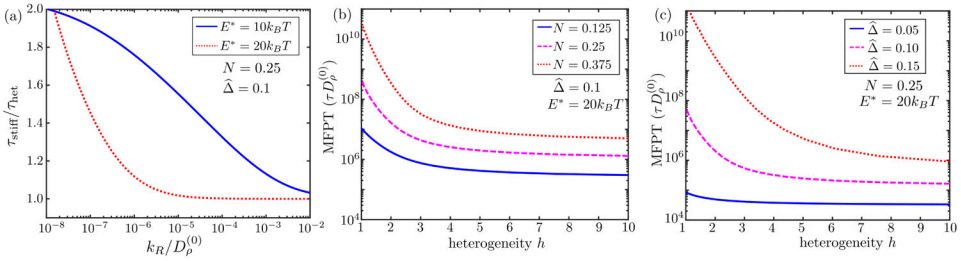

Figure 3.

Chain heterogeneity enhances junction fracture rates when chain end dynamics are slow. (a) Ratio of MFPT to fracture for uniformly stiff ($h = 1$) and heterogeneous ($h = 10$) chains is plotted versus the relative rate of chain end dynamics compared to junction dynamics. (b-c) Time to fragmentation in the limit of infinitely slow chain end dynamics. Dimensionless MFPT is shown as a function of heterogeneity h for (b) chains with a fixed junction length $\widehat{\Delta} = 0.1$ and varying stiffness and (c) chains with a fixed stiffness ($N = 0.25$) but varying junction length. Chains are assumed to start from an equilibrium distribution.

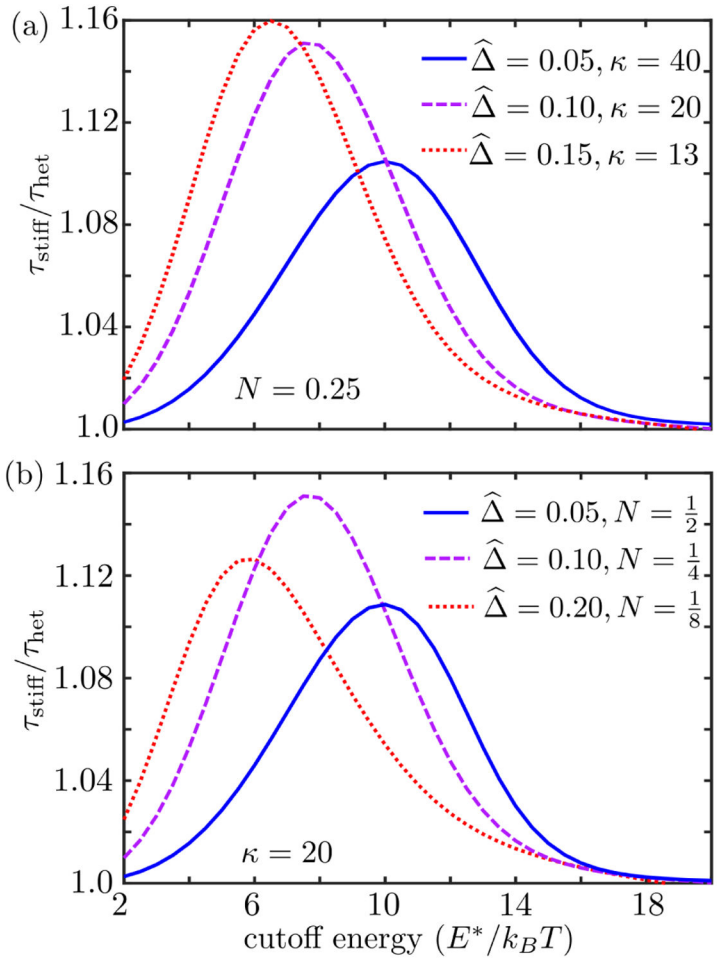

Figure 4.

Enhancement in fracture rate for a heterogeneous vs homogeneous chain with free chain ends. The ratio of MFPT to fracture for a fully stiff chain ($h = 1$) vs a heterogeneous chain ($h = 10$) is plotted as a function of the cutoff energy. (a) Filaments with constant length N but varying junction size and stiffness. (b) Filaments with varying length but constant junction stiffness κ.